Surface dynamics of rough magnetic films

Yu, Tao; Sharma, Sanchar; Blanter, Yaroslav M.; Bauer, Gerrit E.W.

DOI
10.1103/PhysRevB.99.174402

Publication date
2019

Document Version
Final published version

Published in
Physical Review B

Surface dynamics of rough magnetic films

Tao Yu,[1] Sanchar Sharma,[1] Yaroslav M. Blanter,[1] and Gerrit E. W. Bauer[2,1]
[1]*Kavli Institute of NanoScience, Delft University of Technology, 2628 CJ Delft, The Netherlands*
[2]*Institute for Materials Research & WPI-AIMR & CSRN, Tohoku University, Sendai 980-8577, Japan*

(Received 2 February 2019; published 2 May 2019)

The chirality of magnetostatic Damon-Eshbach (DE) magnons affects the transport of energy and angular momentum at the surface of magnetic films and spheres. We calculate the surface-disorder-limited dephasing and transport lifetimes of surface modes of sufficiently thick high-quality ferromagnetic films such as yttrium iron garnet. Surface magnons are not protected by chirality, but interact strongly with smooth surface roughness. Nevertheless, for long-range disorder, the transport is much less affected by the suppressed backscattering (vertex correction). Moreover, in the presence of roughness, ferromagnetic resonance under a *uniform* microwave field can generate a considerable number of surface magnons.

DOI: 10.1103/PhysRevB.99.174402

I. INTRODUCTION

Spin waves or their quanta, magnons, are weakly dissipating carriers of angular momentum and energy [1–5]. Magnetostatic surface or Damon-Eshbach (DE) spin waves in finite-size magnets have additional unique features [6–9] such as exponential localization at the surface of spheres [6] or films [7] and chirality: surface magnons propagate only in one direction that is governed by surface normal and magnetization directions [6–9]. Surface magnons are, for example, found to transport heat in a particular direction, even against a temperature gradient, i.e., heat conveyer-belt effect [10–13]. In spherical magnetic resonators, surface magnons can strongly interact with optical whispering gallery modes [14–17], and the chirality of the DE mode can be beneficial for magnon cooling by light [18].

The physics of surface magnons depends on their lifetime and mean-free path, which are limited by disorder, by phonon and magnon scattering [1–4], and especially by surface roughness [19–22]. As surface magnons are not topologically protected, the effect of chirality on the magnon transport and lifetime in disordered systems has not been thoroughly discussed in the literature. Previous studies [19–21] focused on the damping of the uniform spin precession (the Kittel mode) by two-magnon scattering at surface disorder in either bulk materials [19] or films with nearly zero thickness [20,21]. Recently, scattering of dipole-exchange spin waves by single edge defects in very thin films (80 nm) was studied by numerically solving the linearized Landau-Lifshitz equations, showing a suppression of backscattering of chiral spin waves in the DE configuration, even though the magnetization amplitude is nearly constant over the film [23].

Here we quasi-analytically study lifetime and transport of chiral DE magnons, i.e., for a configuration in which the spin waves propagate normal to an in-plane magnetization, in the presence of surface disorder. We focus on magnetic films/slabs sufficiently thick such that surface states exist, but thin enough to allow interactions between surfaces. We find that the surface roughness strongly reduces the lifetime of magnons, but affects the transport only mildly because of suppressed backscattering. Furthermore, we propose that a uniform magnetic field allows for an efficient population of surface states mediated via the surface roughness. An asymmetry of the surface roughness on the two surfaces of the film [21,24] can lead to an unbalanced excitation of the surface magnons on opposite sides of the sample, which is a necessary conditions for the magnon conveyer belt [10–13].

This paper is organized as follows. We first review the equations that govern the magnon amplitudes or wave functions in Sec. II. In Sec. III, we derive magnon-magnon scattering cross sections by the surface disorder. The lifetime and transport of surface magnons are addressed in Secs. IV and V. Excitation of surface magnons indirectly via Kittel mode is discussed in Sec. VI. We summarize the results and give an outlook in Sec. VII.

II. SURFACE MAGNON WAVE FUNCTION

Magnetostatic waves in ferromagnetic films with in-plane magnetization were studied long back [7,8]. Here, we review the amplitude or the "wave function" of the surface magnons as far as it is relevant for our objectives. As shown in Fig. 1, the surface is perpendicular to the $\hat{\mathbf{x}}$ axis, the equilibrium magnetization points along the $\hat{\mathbf{z}}$ axis, and we are mainly interested in spin waves propagating along the $\hat{\mathbf{y}}$ axis.

The magnetization $\mathbf{M}(\mathbf{r})$ satisfies the Landau-Lifshitz (LL) equation [25]

$$\partial\mathbf{M}(\mathbf{r})/\partial t = -\gamma\mu_0\mathbf{M}(\mathbf{r}) \times \mathbf{H}_{\rm eff}(\mathbf{r}), \tag{1}$$

where γ is modulus of the gyromagnetic ratio, μ_0 denotes the vacuum permeability, and the effective magnetic field

$$\mathbf{H}_{\rm eff}(\mathbf{r}) = -(1/\mu_0)\delta F[\mathbf{M}]/\delta\mathbf{M}(\mathbf{r}), \tag{2}$$

with F being the free energy functional. In the presence of an applied magnetic field $H_z\hat{\mathbf{z}}$ and dipolar interactions,

$$F = -\mu_0 \int d\mathbf{r}\left[M_z H_z + \frac{\mathbf{M}(\mathbf{r})}{8\pi}\cdot\nabla\int d\mathbf{r}'\frac{\nabla'\cdot\mathbf{M}(\mathbf{r}')}{|\mathbf{r}-\mathbf{r}'|}\right]. \tag{3}$$

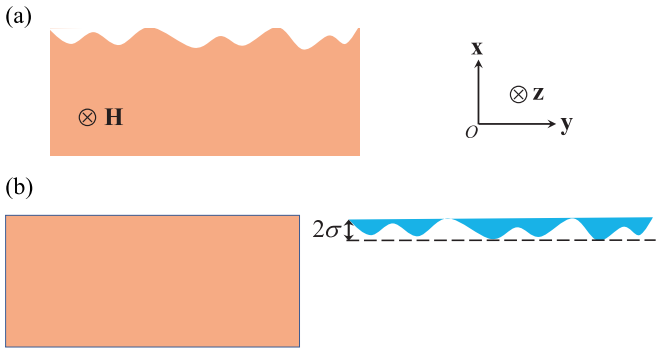

FIG. 1. (a) Surface roughness on the upper surface of a magnetic film. The surface normal is along the $\hat{\mathbf{x}}$-direction. (b) The roughness is located only in a thin surface layer on top of an ordered magnetic film with thickness that corresponds to twice the root-mean-square σ of the thickness fluctuations.

We disregard the crystalline anisotropy and damping, which is often allowed in high-quality materials such as yttrium iron garnet (YIG) [21,26,27]. We ignore the exchange interaction, which is valid for spin waves with wavelengths much larger than the exchange length ∼100 nm in YIG [28].

We linearize Eq. (1) for small magnetization amplitudes around $\mathbf{M} = M_0\hat{\mathbf{z}}$, where M_0 is the saturation magnetization. For a film with in-plane translation symmetry, $\mathbf{M}^{j\mathbf{k}}_{\gamma=x,y} = m^{j\mathbf{k}}_{\gamma}(x)e^{ik_y y}e^{ik_z z}$, where

$$m^{j\mathbf{k}}_{x}(x) = a_{j\mathbf{k}}e^{i\kappa_j x} + b_{j\mathbf{k}}e^{-i\kappa_j x}, \tag{4}$$

$$m^{j\mathbf{k}}_{y}(x) = c_{j\mathbf{k}}e^{i\kappa_j x} + d_{j\mathbf{k}}e^{-i\kappa_j x}. \tag{5}$$

Here, j labels the energy bands of the magnons and $\mathbf{k} = k_y\hat{\mathbf{y}} + k_z\hat{\mathbf{z}}$ represents the in-plane momentum. We choose the normalization condition [6,29]

$$\int d\mathbf{r}\left[M^{j\mathbf{k}}_{x}(\mathbf{r})M^{j\mathbf{k}}_{y}(\mathbf{r})^* - M^{j\mathbf{k}}_{x}(\mathbf{r})^*M^{j\mathbf{k}}_{y}(\mathbf{r})\right] = -i/2, \tag{6}$$

in which M^* is the complex conjugate of M. The coefficients $\{a, b, c, d\}_{j\mathbf{k}}$ are determined using the ansatz $\mathbf{M}^{j\mathbf{k}}_{\gamma} \propto e^{-i\omega_{j\mathbf{k}}t}$ in which $\omega_{j\mathbf{k}}$ is the eigenfrequency. The linearized LL equations are

$$\begin{pmatrix} i\omega_{j\mathbf{k}} - \omega_M\frac{\kappa_j k_y}{k_s^2} & -\omega_H - \omega_M\frac{k_y^2}{k_s^2} \\ \omega_H + \omega_M\frac{\kappa_j^2}{k_s^2} & i\omega_{j\mathbf{k}} + \omega_M\frac{\kappa_j k_y}{k_s^2} \end{pmatrix}\begin{pmatrix} a_{j\mathbf{k}} \\ c_{j\mathbf{k}} \end{pmatrix} = 0, \tag{7}$$

$$\begin{pmatrix} f_+(\mathbf{k}) & f_+^*(\mathbf{k}) \\ f_-^*(\mathbf{k}) & f_-(\mathbf{k}) \end{pmatrix}\begin{pmatrix} a_{j\mathbf{k}} \\ b_{j\mathbf{k}} \end{pmatrix} = 0, \tag{8}$$

where $\omega_H = \gamma\mu_0 H_z$, $\omega_M = \gamma\mu_0 M_0$,

$$f_\pm(\mathbf{k}) = \frac{1}{2}\left(|\mathbf{k}| \pm ik_y\frac{i\omega_{j\mathbf{k}}/\mu_0 - \gamma M_0\kappa_j k_y/k_s^2}{\gamma H_z + \gamma M_0 k_y^2/k_s^2}\right)\frac{e^{i\kappa_j d/2}}{i\kappa_j - |\mathbf{k}|} \tag{9}$$

and $k_s^2 = \kappa_j^2 + |\mathbf{k}|^2$. An equation similar to (7) holds, with $\{a_{j\mathbf{k}}, c_{j\mathbf{k}}, \kappa_j\} \to \{b_{j\mathbf{k}}, d_{j\mathbf{k}}, -\kappa_j\}$. Equation (7) gives the dispersion relation [7]

$$\omega_{j\mathbf{k}} = \sqrt{\omega_H^2 + \omega_H\omega_M\frac{\kappa_j^2 + k_y^2}{k_s^2}}. \tag{10}$$

Equation (8) gives the characteristic equation for κ_j [7],

$$(\beta k_y)^2 + \kappa_j^2(\alpha+1)^2 - |\mathbf{k}|^2 - 2\kappa_j|\mathbf{k}|(\alpha+1)\cot(\kappa_j d) = 0. \tag{11}$$

Here, $\alpha = \omega_H\omega_M/(\omega_H^2 - \omega_{j\mathbf{k}}^2)$ and $\beta = \omega_{j\mathbf{k}}\omega_M/(\omega_H^2 - \omega^2)$.

When $\kappa_j = iq_x$ is purely imaginary, we obtain a DE mode [7]:

$$\begin{aligned} m_x^{\mathbf{k}}(x) &= C[e^{-q_x x}(-\alpha q_x + \beta k_y) + De^{q_x(x+d)}(\alpha q_x + \beta k_y)], \\ m_y^{\mathbf{k}}(x) &= iC[e^{-q_x x}(-\beta q_x + \alpha k_y) + De^{q_x(x+d)}(\beta q_x + \alpha k_y)], \end{aligned} \tag{12}$$

in which C is governed by the normalization Eq. (6); d denotes the thickness of the film, and

$$D = \frac{q_x(\alpha+1) - \beta k_y + |\mathbf{k}|}{q_x(\alpha+1) + \beta k_y - |\mathbf{k}|}. \tag{13}$$

The characteristic relation for this DE mode becomes [7]

$$(\beta k_y)^2 - q_x^2(\alpha+1)^2 - |\mathbf{k}|^2 - 2q_x|\mathbf{k}|(\alpha+1)\coth(q_x d) = 0. \tag{14}$$

For surface magnons with $k_y < 0$ and $e^{q_x d} \gg 1$,

$$im_x^{\mathbf{k}} + \frac{k_y}{|\mathbf{k}|}m_y^{\mathbf{k}} \approx 0, \tag{15}$$

i.e., when $\mathbf{k} = k_y\hat{\mathbf{y}}$ the DE magnons are circularly polarized. When $k_z \neq 0$, the DE modes precess elliptically. From Eq. (14) we conclude that DE modes preserve their character as long as $|k_z| < |k_y|\sqrt{M_0/H_z}$ [7]. We now prove that for small k_z the ellipticity is weak**.** When $e^{q_x d} \gg 1$, $\coth(q_x d) \to 1$ and Eq. (14) simplifies to

$$q_x(\alpha+1) + |\mathbf{k}| \approx |\beta k_y| = \beta k_y, \tag{16}$$

because $\beta, k_y < 0$. This implies $D \to 0$ in Eq. (13). Therefore

$$\begin{aligned} im_x^{\mathbf{k}} + \frac{k_y}{|\mathbf{k}|}m_y^{\mathbf{k}} &\to iCe^{-q_x x}\left[-\alpha q_x + \beta k_y + \frac{k_y}{|\mathbf{k}|}(-\beta q_x + \alpha k_y)\right] \\ &= \frac{iCe^{-q_x x}}{|\mathbf{k}|}\left[|\mathbf{k}|^2 - (\alpha+1)q_x^2 + \alpha k_y^2\right] = 0, \end{aligned} \tag{17}$$

where the term in the last square bracket vanishes because of the dispersion relation (10). This relation is essential for the chiral coupling between the magnons and surface roughness as discussed in Sec. III.

III. MAGNON–SURFACE-ROUGHNESS INTERACTION

We focus on a simple generic model of surface roughness: the magnetic order is preserved up to the surface position, which varies slightly as a function of position in a random manner. A film with surface roughness [Fig. 1(a)] can be separated into two parts: a smooth film and a fluctuating thin surface layer [19–22], as shown in Fig. 1(b).

The free energy in Eq. (3) is affected by the surface morphology. We derive the two-magnon scattering amplitude induced by the dipolar interaction and the Zeeman energy.

A. Dipolar interaction

The free energy due to the dipolar interaction in the magnetic film [25],

$$F_d = -\frac{\mu_0}{2}\int d\mathbf{r}_\parallel \int_{-\frac{d}{2}+x_l(\mathbf{r}_\parallel)}^{\frac{d}{2}+x_u(\mathbf{r}_\parallel)} dx\, \mathbf{M}(\mathbf{r})\cdot\mathbf{H}_D(\mathbf{r}), \tag{18}$$

where $\mathbf{r}_\parallel = y\hat{\mathbf{y}} + z\hat{\mathbf{z}}$. $x_u(\mathbf{r}_\parallel)$ and $x_l(\mathbf{r}_\parallel)$ are the fluctuating part of the upper and lower surface positions, respectively. The magnetic potential ψ, defined in terms of the demagnetization field as $\mathbf{H}_D = -\nabla\psi$, can be written as Coulomb-like expression [25],

$$\psi(\mathbf{r}) = -\int_V d\mathbf{r}' \frac{\nabla\cdot\mathbf{M}(\mathbf{r}')}{4\pi|\mathbf{r}-\mathbf{r}'|}. \tag{19}$$

The free energy reads

$$F_d = -\frac{\mu_0}{8\pi}\int d\mathbf{r}_\parallel \int_{-\frac{d}{2}+x_l(\mathbf{r}_\parallel)}^{\frac{d}{2}+x_u(\mathbf{r}_\parallel)} dx \int d\mathbf{r}'_\parallel \int_{-\frac{d}{2}+x_l(\mathbf{r}'_\parallel)}^{\frac{d}{2}+x_u(\mathbf{r}'_\parallel)} dx' \times M_\beta(\mathbf{r})\partial_\beta\partial_\alpha \frac{M_\alpha(\mathbf{r}')}{|\mathbf{r}-\mathbf{r}'|}, \tag{20}$$

using the summation convention over repeated Cartesian indices $\alpha = \{x, y, z\}$. When the amplitudes of $x_u(\mathbf{r}_\parallel)$ and $x_l(\mathbf{r}_\parallel)$ are much smaller than both thickness of the film and decay depth of the DE modes, we can simplify Eq. (20) by the *mean-value theorem* for the integral, i.e.,

$$\int_{d/2}^{d/2+x_u} f(x)dx \approx f\left(\frac{d}{2}\right)x_u. \tag{21}$$

To linear order, $F_d = F_0 + F_d^u + F_d^l$, where F_0 is given by Eq. (20), putting $x_u = x_l = 0$,

$$F_d^u = -\frac{\mu_0}{4\pi}\int d\mathbf{r}_\parallel \int_{-\frac{d}{2}}^{\frac{d}{2}} dx\, M_\beta(\mathbf{r})\partial_\beta\partial_\alpha \int d\mathbf{r}'_\parallel x_u(\mathbf{r}'_\parallel) \times \frac{M_\alpha(d/2, \mathbf{r}'_\parallel)}{\sqrt{(x-d/2)^2 + (\mathbf{r}_\parallel - \mathbf{r}'_\parallel)^2}}, \tag{22}$$

and

$$F_d^l = \frac{\mu_0}{4\pi}\int d\mathbf{r}_\parallel \int_{-\frac{d}{2}}^{\frac{d}{2}} dx\, M_\beta(\mathbf{r})\partial_\beta\partial_\alpha \int d\mathbf{r}'_\parallel x_l(\mathbf{r}'_\parallel) \times \frac{M_\alpha(-d/2, \mathbf{r}'_\parallel)}{\sqrt{(x+d/2)^2 + (\mathbf{r}_\parallel - \mathbf{r}'_\parallel)^2}}. \tag{23}$$

Note that this approximation does not take into account the large-momentum scattering that is caused by the derivative of $x_{u/l}(\mathbf{r}_\parallel)$. Our theory is therefore limited to the smooth surface roughness that governs the Gilbert damping [21].

These expressions can be integrated with the Hamiltonian formulation for the magnetization dynamics [8,17,30–32]. Substituting $\mathbf{M} \to -\gamma\hbar\hat{\mathbf{S}}$ (and $M_0 = \gamma\hbar S$), the Hamiltonian for the upper surface roughness reads [8,17,30–32]

$$H_{\rm d}^u = -\frac{\mu_0\gamma^2\hbar^2}{4\pi}\int d\mathbf{r}\int d\mathbf{r}'_\parallel (\hat{S}_x(\mathbf{r})\hat{S}_y(\mathbf{r})\hat{S}_z(\mathbf{r})) \times \hat{\mathbf{G}}\left(x-\frac{d}{2}, \mathbf{r}_\parallel - \mathbf{r}'_\parallel\right) \times \left(\hat{S}_x\left(\frac{d}{2}, \mathbf{r}'_\parallel\right), \hat{S}_y\left(\frac{d}{2}, \mathbf{r}'_\parallel\right), \hat{S}_z\left(\frac{d}{2}, \mathbf{r}'_\parallel\right)\right)^T, \tag{24}$$

introducing the Green function tensor [33]

$$\hat{\mathbf{G}}\left(x-\frac{d}{2}, \mathbf{r}_\parallel - \mathbf{r}'_\parallel\right) \equiv \begin{pmatrix} \partial_x^2 & \partial_x\partial_y & \partial_x\partial_z \\ \partial_y\partial_x & \partial_y^2 & \partial_y\partial_z \\ \partial_z\partial_x & \partial_z\partial_y & \partial_z^2 \end{pmatrix} \times \frac{x_u(\mathbf{r}'_\parallel)}{\sqrt{(x-\frac{d}{2})^2 + (\mathbf{r}_\parallel - \mathbf{r}'_\parallel)^2}}. \tag{25}$$

We focus on the linear regime, thereby disregarding higher-order terms encoding the magnon-magnon scattering process that becomes important for large magnon numbers [34,35]. The spin operators may then be expressed in terms of magnon operators $\hat{\alpha}_{j\mathbf{k}}$ [17,30–32],

$$\hat{S}_{x,y}(\mathbf{r}) = \sqrt{2S}\sum_{j,\mathbf{k}}\left[M_{x,y}^{j\mathbf{k}}(\mathbf{r})\hat{\alpha}_{j\mathbf{k}} + M_{x,y}^{j\mathbf{k}}(\mathbf{r})^*\hat{\alpha}_{j\mathbf{k}}^\dagger\right],$$
$$\hat{S}_z(\mathbf{r}) = -S + (\hat{S}_x^2 + \hat{S}_y^2)/(2S). \tag{26}$$

The interaction for the upper surface then reduces to

$$H_{\rm d}^u = \sum_{j\mathbf{k}}(L_{j\mathbf{k}}\hat{\alpha}_{j\mathbf{k}} + \text{H.c.}) + \sum_{j\mathbf{k}}\sum_{j'\mathbf{k}'}[A_{j\mathbf{k},j'\mathbf{k}'}\hat{\alpha}_{j\mathbf{k}}\hat{\alpha}_{j'\mathbf{k}'} + B_{j\mathbf{k},j'\mathbf{k}'}\hat{\alpha}_{j\mathbf{k}}^\dagger\hat{\alpha}_{j'\mathbf{k}'} + C_{j\mathbf{k},j'\mathbf{k}'}\hat{\alpha}_{j\mathbf{k}}^\dagger\hat{\alpha}_{j'\mathbf{k}'}^\dagger + D_{j\mathbf{k},j'\mathbf{k}'}\hat{\alpha}_{j\mathbf{k}}\hat{\alpha}_{j'\mathbf{k}'}^\dagger]. \tag{27}$$

The coefficients of the linear term,

$$L_{j\mathbf{k}} = -\mu_0 M_0\sqrt{\frac{\hbar\gamma M_0}{2}}x_u(-\mathbf{k})k_z \times \int dx\, e^{(x-\frac{d}{2})|\mathbf{k}|}\left[im_x^{j\mathbf{k}}(x) + \frac{k_y}{|\mathbf{k}|}m_y^{j\mathbf{k}}(x)\right], \tag{28}$$

nearly vanish for DE modes with momenta $k_y\hat{\mathbf{y}} + k_z\hat{\mathbf{z}} = -|k_y|\hat{\mathbf{y}} + k_z\hat{\mathbf{z}}$ when $|\mathbf{k}|d \gtrsim 1$ because of Eq. (15).

The linear terms do not conserve spin and therefore exert a torque on the magnetization [$\mathbf{M}_0(\mathbf{r}) = M_0\hat{\mathbf{z}}$ for a clean surface]. When the linear term is eliminated by the transformation $\hat{\alpha}_{j\mathbf{k}}^\dagger \to \hat{\alpha}_{j\mathbf{k}}^\dagger - L_{j\mathbf{k}}/\omega_{j\mathbf{k}}$, Eq. (26) introduces transverse components of the equilibrium magnetization,

$$\mathbf{M}_{x,y}^0(\mathbf{r}) = \sqrt{2M_0\gamma\hbar}\sum_{j,\mathbf{k}}\left[\frac{M_{x,y}^{j\mathbf{k}}(\mathbf{r})L_{j\mathbf{k}}^*}{\omega_{j\mathbf{k}}} + \text{H.c.}\right]. \tag{29}$$

Strong surface disorder therefore affects the equilibrium magnetization and eigenmodes. However, here we focus on weak disorder with $|\mathbf{M}_{x,y}^0(\mathbf{r})| \ll M_0$, where we may disregard the linear term.

The quadratic terms in $H_{\rm d}^u$ represent two-magnon scattering by disorder, with coefficients

$$A_{j\mathbf{k},j'\mathbf{k}'} = -\mu_0\gamma\hbar M_0 x_u(-\mathbf{k}-\mathbf{k}')\Bigg\{\int dx\, e^{(x-\frac{d}{2})|\mathbf{k}|}\begin{pmatrix} m_x^{j\mathbf{k}}(x) & m_y^{j\mathbf{k}}(x)\end{pmatrix}\begin{pmatrix} |\mathbf{k}| & -ik_y \\ -ik_y & -\frac{k_y^2}{|\mathbf{k}|}\end{pmatrix}\begin{pmatrix} m_x^{j'\mathbf{k}'}(\frac{d}{2}) \\ m_y^{j'\mathbf{k}'}(\frac{d}{2})\end{pmatrix}$$
$$+\frac{1}{2}\frac{(k_z+k_z')^2}{|\mathbf{k}+\mathbf{k}'|}\int dx\big[m_x^{j\mathbf{k}}(x)m_x^{j'\mathbf{k}'}(x)+m_y^{j\mathbf{k}}(x)m_y^{j'\mathbf{k}'}(x)\big]e^{(x-\frac{d}{2})|\mathbf{k}+\mathbf{k}'|}-2m_x^{j\mathbf{k}}(d/2)m_x^{j'\mathbf{k}'}(d/2)\Bigg\}, \tag{30}$$

and

$$B_{j\mathbf{k},j'\mathbf{k}'} = -\mu_0\gamma\hbar M_0 x_u(\mathbf{k}-\mathbf{k}')\Bigg\{\int dx\, e^{(x-\frac{d}{2})|\mathbf{k}|}\begin{pmatrix} m_x^{j\mathbf{k}}(x)^* & m_y^{j\mathbf{k}}(x)^*\end{pmatrix}\begin{pmatrix} |\mathbf{k}| & ik_y \\ ik_y & -\frac{k_y^2}{|\mathbf{k}|}\end{pmatrix}\begin{pmatrix} m_x^{j'\mathbf{k}'}(\frac{d}{2}) \\ m_y^{j'\mathbf{k}'}(\frac{d}{2})\end{pmatrix}$$
$$+\frac{1}{2}\frac{(k_z-k_z')^2}{|\mathbf{k}-\mathbf{k}'|}\int dx\big[m_x^{j\mathbf{k}}(x)^*m_x^{j'\mathbf{k}'}(x)+m_y^{j\mathbf{k}}(x)^*m_y^{j'\mathbf{k}'}(x)\big]e^{(x-\frac{d}{2})|\mathbf{k}-\mathbf{k}'|}-2m_x^{j\mathbf{k}}(d/2)^*m_x^{j'\mathbf{k}'}(d/2)\Bigg\}. \tag{31}$$

$C_{j\mathbf{k},j'\mathbf{k}'} = A^*_{j\mathbf{k},j'\mathbf{k}'}$ and $D_{j\mathbf{k},j'\mathbf{k}'} = B^*_{j\mathbf{k},j'\mathbf{k}'}$ by hermiticity.

The first and nonlocal term in Eq. (31) couples two DE states with opposite momenta only very weakly, because of their (nearly) circular polarization $m_x^{j\mathbf{k}}(x)^* + i\frac{k_y}{|\mathbf{k}|}m_x^{j\mathbf{k}}(x)^* \approx 0$ when $k_y < 0$ and $|k_z| < |k_y|\sqrt{M_0/H_z}$ [see Eq. (15)], and may therefore be disregarded. The local second and third terms are exponentially suppressed because of the low overlap of the magnons with opposite momenta that are localized on opposite surfaces. The large momentum backscattering of DE magnons by surface disorder is therefore suppressed. Similar results hold for the lower surface by $k_y \to -k_y$ and $d/2 \to -d/2$.

B. Zeeman energy

The free energy due to the Zeeman interaction is [25]

$$F_Z = -\mu_0\int d\mathbf{r}_\parallel \int_{-d/2+x_l(\mathbf{r}_\parallel)}^{d/2+x_u(\mathbf{r}_\parallel)} dx \mathbf{M}(\mathbf{r})\cdot\mathbf{H}_z, \tag{32}$$

and the equivalent (quantum) Hamiltonian reads

$$H_Z = \frac{\mu_0\gamma\hbar}{2S}\int d\mathbf{r}_\parallel \int_{-d/2+x_l(\mathbf{r}_\parallel)}^{d/2+x_u(\mathbf{r}_\parallel)} \big[\hat{S}_x^2(\mathbf{r})+\hat{S}_y^2(\mathbf{r})\big]H_z dx. \tag{33}$$

As above, we derive the interaction Hamiltonian with small surface roughness:

$$H_Z^u = \frac{\mu_0\gamma^2\hbar^2}{2M_0}H_z\int d\mathbf{r}_\parallel\left[\hat{S}_x^2\left(\frac{d}{2},\mathbf{r}_\parallel\right)+\hat{S}_y^2\left(\frac{d}{2},\mathbf{r}_\parallel\right)\right]x_u(\mathbf{r}_\parallel), \tag{34}$$

$$H_Z^l = -\frac{\mu_0\gamma^2\hbar^2}{2M_0}H_z\int d\mathbf{r}_\parallel\left[\hat{S}_x^2\left(\frac{d}{2},\mathbf{r}_\parallel\right)+\hat{S}_y^2\left(\frac{d}{2},\mathbf{r}_\parallel\right)\right]x_l(\mathbf{r}_\parallel). \tag{35}$$

By the Bogoliubov transformation (26), the interaction Hamiltonian by a rough upper surface becomes

$$H_Z^u = \sum_{j\mathbf{k}}\sum_{j'\mathbf{k}'}[\tilde{A}_{j\mathbf{k},j'\mathbf{k}'}\hat{\alpha}_{j\mathbf{k}}\hat{\alpha}_{j'\mathbf{k}'}+\tilde{B}_{j\mathbf{k},j'\mathbf{k}'}\hat{\alpha}^\dagger_{j\mathbf{k}}\hat{\alpha}_{j'\mathbf{k}'}$$
$$+\tilde{C}_{j\mathbf{k},j'\mathbf{k}'}\hat{\alpha}^\dagger_{j\mathbf{k}}\hat{\alpha}^\dagger_{j'\mathbf{k}'}+\tilde{D}_{j\mathbf{k},j'\mathbf{k}'}\hat{\alpha}_{j\mathbf{k}}\hat{\alpha}^\dagger_{j'\mathbf{k}'}], \tag{36}$$

in which

$$\tilde{A}_{j\mathbf{k},j'\mathbf{k}} = \mu_0\gamma\hbar H_z x_u(-\mathbf{k}-\mathbf{k}')\sum_{\gamma=x,y} m_\gamma^{j\mathbf{k}}\left(\frac{d}{2}\right)m_\gamma^{j'\mathbf{k}'}\left(\frac{d}{2}\right),$$
$$\tilde{B}_{j\mathbf{k},j'\mathbf{k}} = \mu_0\gamma\hbar H_z x_u(\mathbf{k}-\mathbf{k}')\sum_{\gamma=x,y} m_\gamma^{j\mathbf{k}}\left(\frac{d}{2}\right)^* m_\gamma^{j'\mathbf{k}'}\left(\frac{d}{2}\right). \tag{37}$$

The fluctuations in the Zeeman energy are generated only by the states with significant wave functions on the rough surface. Similar result holds for the lower surface, with $k_y \to -k_y$ and $d/2 \to -d/2$.

IV. SURFACE DAMPING

We now use the Hamiltonians derived in the previous section to find the damping of surface magnons by rough surfaces, i.e., the lifetime for a surface magnon to reside at particular states. We first use the Green's function technique, and subsequently discuss the results.

A. Analytical analysis

The Green function of a magnon in the jth band with in-plane wave vector $\mathbf{k}$ is [36–38]

$$G_{j\mathbf{k}}(\omega) = \frac{1}{\omega-\omega_{j\mathbf{k}}+i\Gamma_{j\mathbf{k}}-\Sigma_{j\mathbf{k}}(\omega)}, \tag{38}$$

where $\omega_{j\mathbf{k}}$ is the resonance frequency, $\Sigma_{j\mathbf{k}}(\omega)$ is the self-energy due to surface scattering, $\Gamma_{j\mathbf{k}} = \alpha_0\omega_{j\mathbf{k}}$ is the intrinsic damping in the absence of surface roughness, and α_0 is the Gilbert damping constant [39] of the Kittel mode of a film with smooth surfaces. The imaginary part of Σ governs the magnon scattering rate or damping due to the surface roughness

$$\alpha_s(\omega_{j\mathbf{k}}) \equiv -2\,\mathrm{Im}\Sigma(\omega_{\mathbf{k}})/\omega_{\mathbf{k}}. \tag{39}$$

In the Matsubara representation [36–38],

$$G_{j\mathbf{k}}(\tau-\tau') = -\left\langle T_\tau\hat{\alpha}_{j\mathbf{k}}(\tau)\hat{\alpha}^\dagger_{j\mathbf{k}}(\tau')\exp\left(-\int_0^\beta d\tilde{\tau}H_{\rm int}^s\right)\right\rangle, \tag{40}$$

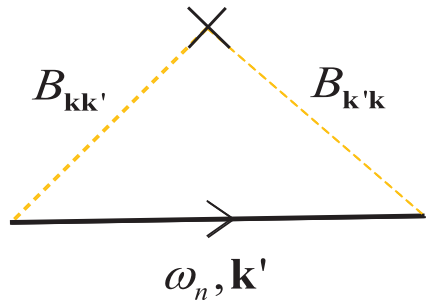

FIG. 2. Feynman diagram for the self-energy in the self-consistent Born approximation. Here, → represents the full Green function $G_{j\mathbf{k}}(i\omega_n)$. The orange dashed line denotes the scattering potential.

where $\beta = 1/(k_B T)$ and T is the temperature. T_τ is the chronological product with imaginary time τ. $H^u_{\rm int}$ is the interaction Hamiltonian due to the surface roughness at the upper layer,

$$H^u_{\rm int} = \sum_{j\mathbf{k}} \sum_{j'\mathbf{k}'} [\mathcal{A}_{j\mathbf{k},j'\mathbf{k}'} \hat{\alpha}_{j\mathbf{k}} \hat{\alpha}_{j'\mathbf{k}'} + \mathcal{B}_{j\mathbf{k},j'\mathbf{k}'} \hat{\alpha}^\dagger_{j\mathbf{k}} \hat{\alpha}_{j'\mathbf{k}'}] + \text{H.c.}, \tag{41}$$

in which $\mathcal{A}_{j\mathbf{k},j'\mathbf{k}'} = A_{j\mathbf{k},j'\mathbf{k}'} + \tilde{A}_{j\mathbf{k},j'\mathbf{k}'}$ and $\mathcal{B}_{j\mathbf{k},j'\mathbf{k}'} = B_{j\mathbf{k},j'\mathbf{k}'} + \tilde{B}_{j\mathbf{k},j'\mathbf{k}'}$. In the *weak* coupling regime, the Green function in the frequency-momentum space $G_{j\mathbf{k}}(i\omega_n) = \int_0^\beta d\tau\, e^{i\omega_n \tau} G_{j\mathbf{k}}(\tau)$ can be expanded in the *self-consistent* Born approximation [40–42] as

$$G_{j\mathbf{k}}(i\omega_n) = G^{(0)}_{j\mathbf{k}}(i\omega_n) + G^{(0)}_{j\mathbf{k}}(i\omega_n) \Bigg\{ \sum_{j'\mathbf{k}'} |\mathcal{B}_{j'\mathbf{k}',j\mathbf{k}}|^2 \times G_{j'\mathbf{k}'}(i\omega_n) + \sum_{j'\mathbf{k}'} |\mathcal{A}_{j'\mathbf{k}',j\mathbf{k}}|^2 G_{j'\mathbf{k}'}(-i\omega_n) \Bigg\} \times G_{j\mathbf{k}}(i\omega_n), \tag{42}$$

where $G^{(0)}_{j\mathbf{k}}(i\omega_n) = 1/(i\omega_n - \omega_{j\mathbf{k}} + i\Gamma_{j\mathbf{k}})$. The corresponding Feynman diagram for the self-energy due to the surface scattering is shown in Fig. 2.

In the real frequency domain, by the analytical continuation $i\omega_n \to \omega + i\delta$, the self-energy of the magnons from the surface roughness is calculated to be

$$\Sigma_{j\mathbf{k}}(\omega) = \sum_{j'\mathbf{k}'} |\mathcal{B}_{j\mathbf{k},j'\mathbf{k}'}|^2 \frac{G^{(0)}_{j'\mathbf{k}'}(\omega)}{1 - G^{(0)}_{j'\mathbf{k}'}(\omega)\Sigma_{j'\mathbf{k}'}(\omega)} + \sum_{j'\mathbf{k}'} |\mathcal{A}_{j\mathbf{k},j'\mathbf{k}'}|^2 \frac{G^{(0)}_{j'\mathbf{k}'}(-\omega)}{1 - G^{(0)}_{j'\mathbf{k}'}(-\omega)\Sigma_{j'\mathbf{k}'}(-\omega)}. \tag{43}$$

At the magnon's frequency $\omega = \omega_{j\mathbf{k}}$,

$$\Sigma_{j\mathbf{k}}(\omega_{j\mathbf{k}}) = \sum_{j'\mathbf{k}'} |\mathcal{B}_{j\mathbf{k},j'\mathbf{k}'}|^2 \frac{G^{(0)}_{j'\mathbf{k}'}(\omega_{j\mathbf{k}})}{1 - G^{(0)}_{j'\mathbf{k}'}(\omega_{j\mathbf{k}})\Sigma_{j'\mathbf{k}'}(\omega_{j\mathbf{k}})} + \sum_{j'\mathbf{k}'} |\mathcal{A}_{j\mathbf{k},j'\mathbf{k}'}|^2 \frac{G^{(0)}_{j'\mathbf{k}'}(-\omega_{j\mathbf{k}})}{1 - G^{(0)}_{j'\mathbf{k}'}(-\omega_{j\mathbf{k}})\Sigma_{j'\mathbf{k}'}(-\omega_{j\mathbf{k}})}. \tag{44}$$

The $\mathcal{A}$ term is off-resonant, with negligible contribution to the self-energy since $\omega_{j\mathbf{k}} + \omega_{j'\mathbf{k}'} \gg \Gamma_{j'\mathbf{k}'}$ in $G^{(0)}_{j'\mathbf{k}'}(-\omega_{j\mathbf{k}})$. Hence, in the calculation below, we disregard this contribution, which is the "rotating wave approximation" [35,43,44]. Using Eq. (31), $|\mathcal{B}_{j\mathbf{k},j'\mathbf{k}'}|^2 \propto x_{u,l}(\mathbf{k} - \mathbf{k}') x_{u,l}(\mathbf{k}' - \mathbf{k})$ and, under the ergodic hypothesis, a configurational averaging of $\Sigma_{j\mathbf{k}}$ over the disorder leads to a self-correlation function that we model by a Gaussian [21,24],

$$\langle x_{u,l}(\mathbf{k}) x_{u,l}(-\mathbf{k}) \rangle = \pi R^2_{u,l} \sigma^2_{u,l} \exp\left(-|\mathbf{k}|^2 R^2_{u,l}/4\right), \tag{45}$$

in which σ and R are the root mean square (rms) of the amplitude and correlation length of the surface roughness, respectively.

B. Results

Concrete predictions for the magnon damping in a specific material require knowledge of the sample and material parameters. We focus on a YIG film with $\mu_0 M_0 = 0.177$ T [26,27,45], $\alpha_0 = 5 \times 10^{-5}$ [45,46], and $d = 3$ μm. The surface topology of YIG can be varied by different polishing methods [47]. Varying σ from several nm and correlation lengths R of the order micrometers, strongly affects the transverse spin Seebeck effect. However, here we focus on longitudinal (in-plane) transport. We adopt here the smooth surface roughness with $R = 2$ μm, $\sigma_u = 4$ nm as reported for ferromagnetic metal films [21,47]. The interface to the substrate gallium gadolinium garnet (GGG) is believed to be of very high quality, so we disregard any interface roughness of the lower surface, i.e., we adopt $\sigma_l = 0$. The choice for a long-range surface roughness implies that magnetostatic magnons cannot be scattered into (degenerate) exchange-regime magnons with high momentum, which are therefore disregarded in the following.

The dispersion relations of the surface and bulk modes of magnetic films can be found in Fig. 3 in Ref. [7] and textbooks. DE modes are allowed for finite k_z as long as $|k_z/k_y| < \sqrt{M_0/H_z}$ and frequencies above the magnetostatic spin-wave band, $\omega > \gamma\mu_0\sqrt{H_z^2 + M_0 H_z}$ [7]. We focus here on DE magnons with $k_z = 0$ and $|k_y| d > 1/2$ that are exponentially localized near the surface and frequencies approaching the limiting constant $\gamma\mu_0(H_z + M_0/2)$ [8] (see also Sec. II). These magnons are spectrally distant from the magnetostatic spin-wave band [7,8], which therefore do not contribute to the self-energy of the surface magnons by two-magnon scattering; see Eq. (44).

Figure 3 shows a plot of the effective scattering potential $|\mathcal{B}_{j\mathbf{k}j\mathbf{k}'}|$ [defined below Eq. (41)], where index j is that of the DE band, between a DE mode with momentum $\mathbf{k}' = (1/d)\hat{\mathbf{y}}$ and DE modes with momentum $\mathbf{k}$ for in-plane magnetic field $H_z = M_0$ and correlation function Eq. (45).

The rough upper surface scatters magnons with positive momentum into magnons on the same surface, while backscattering to magnons on the remote surface is suppressed, for larger k almost completely. The phase space for scattering is defined by the white and blue boundary $k_z = \sqrt{H_z/M_0} k_y$, the point of degeneracy of the DE and bulk modes. We observe that the scattering is dominated by small momentum transfer $|\mathbf{k} - \mathbf{k}'| \lesssim 2/R$. Since the frequency is conserved for two-magnon scattering, we plot the isofrequency

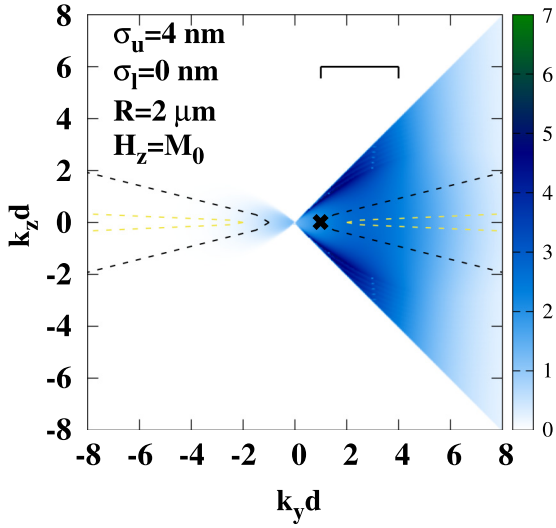

FIG. 3. Momentum $\mathbf{k}$ dependence of the scattering potential $|\mathcal{B}_{\mathbf{k}\mathbf{k}'}|$ (in units of $10^{-8}\mu_0\gamma M_0$) between DE modes. $\mathbf{k}'$ is fixed to $(1/d)\hat{\mathbf{y}}$, i.e., the cross in the figure. The black and orange dashed curves represent the equal-frequency contours for magnons with momentum $\mathbf{k}' = (1/d)\hat{\mathbf{y}}$ and $(2/d)\hat{\mathbf{y}}$, respectively. d is the film thickness, $\sigma_{u/l}$ the rms amplitude (upper/lower surface), and R the correlation length of the surface roughness. The horizontal bar indicates $2d/R$.

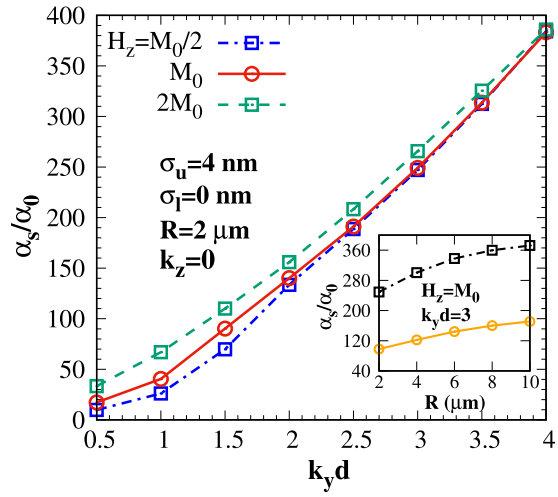

FIG. 4. Momentum dependence of surface damping coefficient α_s relative to the intrinsic Gilbert damping $\alpha_0 = 5\times10^{-5}$. The applied magnetic fields are $H_z = M_0/2$ (blue dashed-dotted curve with squares), M_0 (red solid curve with circles) and $2M_0$ (green dashed curve with squares), respectively. Inset: Correlation length R dependence of α_s for $H_z = M_0$ and $k_y d = 3$. The black dot-dashed curve with squares and the solid curve with circles are calculated with $\sigma_u = 4$ μm and 2 μm, respectively.

contours for the magnons with momentum $\mathbf{k}' = (1/d)\hat{\mathbf{y}}$ (black) and $(2/d)\hat{\mathbf{y}}$ (orange) respectively, illustrating that with larger momentum the magnons are increasingly scattered in the forward direction, reflecting the "ridge"-like energy spectra of DE magnons [7]. This feature allows simplifications of the analysis of DE magnon surface damping and transport (see Sec. V) below.

As discussed above, DE magnons with momentum $\mathbf{k} = |k_y|\hat{\mathbf{y}}$ can only scatter into other DE magnons. We find the surface damping coefficient from the self-energy by self-consistently solving the integral equations [42] (omitting the constant band index)

$$\Sigma_{\mathbf{k}}(\omega_{\mathbf{k}}) = \sum_{\mathbf{k}'} |\mathcal{B}_{\mathbf{k}\mathbf{k}'}|^2 \frac{G^{(0)}_{\mathbf{k}'}(\omega_{\mathbf{k}})}{1 - G^{(0)}_{\mathbf{k}'}(\omega_{\mathbf{k}})\Sigma_{\mathbf{k}'}(\omega_{\mathbf{k}})}$$
$$\approx \sum_{\mathbf{k}'} |\mathcal{B}_{\mathbf{k}\mathbf{k}'}|^2 \frac{G^{(0)}_{\mathbf{k}'}(\omega_{\mathbf{k}})}{1 - G^{(0)}_{\mathbf{k}'}(\omega_{\mathbf{k}})\Sigma_{\mathbf{k}}(\omega_{\mathbf{k}})}. \quad (46)$$

In the last step, we invoke the long-range nature of the scattering potential $|\mathcal{B}_{\mathbf{k}\mathbf{k}'}|^2 \propto e^{-|\mathbf{k}-\mathbf{k}'|^2R^2/4}$ that allows us to replace the self-energy $\Sigma_{\mathbf{k}'}(\omega_{\mathbf{k}})$ by $\Sigma_{\mathbf{k}}(\omega_{\mathbf{k}})$. Equation (46) is numerically solved by carrying out the integral of $\mathbf{k}'$ explicitly.

The long-range nature of the scattering potential implies localization of the scattering in momentum space with the analytical estimate

$$\Sigma_{\mathbf{k}}(\omega_{\mathbf{k}}) \approx \frac{|\mathcal{B}_{\mathbf{k}\mathbf{k}}|^2}{i\Gamma_{\mathbf{k}} - \Sigma_{\mathbf{k}}(\omega_{\mathbf{k}})} \frac{L^2}{4\pi^2} S, \quad (47)$$

where L^2 is the sample area and

$$S \approx \frac{2\sqrt{H_z/M_0}}{2\pi}\pi\left(\frac{2}{R}\right)^2 = \frac{4\sqrt{H_z/M_0}}{R^2} \quad (48)$$

denotes the scattering area in reciprocal space (see Fig. 3). Disregarding the small intrinsic Gilbert damping α_0 and the real part of the self-energy, we find

$$|\mathrm{Im}\,\Sigma_{\mathbf{k}}| \approx \frac{L}{\pi R}|\mathcal{B}_{\mathbf{k}\mathbf{k}}|\left(\frac{H_z}{M_0}\right)^{1/4}. \quad (49)$$

$|\mathcal{B}_{\mathbf{k}\mathbf{k}}| \propto k\sigma R/L$ implies that $\mathrm{Im}\,\Sigma_{\mathbf{k}} \propto \sigma k_y$ but does not depend on R. When $H_z = M_0$, and $k_y d = 2$ ($k_y d = 3$), $\alpha_s = 5.67\times10^{-3}$ (0.84×10^{-2}) which is of the same order of magnitude as the numerical results $\alpha_s = 7.0\times10^{-3}$ (1.24×10^{-2}).

Figure 4 is a plot of the k_y and in-plane magnetic field dependence of the calculated surface damping coefficient α_s that is normalized by the intrinsic Gilbert damping $\alpha_0 = 5\times10^{-5}$, confirming the approximate linear dependence $\alpha_s \propto \sigma k_y$ derived above, for larger momenta $k_y d \gtrsim 2$ and $\mathbf{k} = k_y\hat{\mathbf{y}}$. Physically, this effect is caused by the increasing localization of the wave functions at the surface, which becomes more susceptible to the roughness, while simultaneously the phase space for scattering increases. The enhanced surface damping coefficient for larger wave numbers $k_y d \gtrsim 2.5$ is of the order of 0.01, much larger than the Gilbert damping in YIG, which should hinder the spectroscopic observation of DE modes [48–50] as well as the manipulation of magnons by light [18].

At large momenta, the coupling strength between DE modes, determined by the amplitude overlap at the sample surface, $|\mathcal{B}_{\mathbf{k}\mathbf{k}'}|^2 \propto kk'$ increases significantly [see Eqs. (31) and (37)], reflecting their increased surface localization. At large momenta (or strong surface roughness), the self-consistent Born approximation breaks down [38,40–42]. The more involved single-site approximation could then be used [51], but we note that the divergence for large wave numbers is an artifact of the magnetostatic approximation: the

exchange interaction eventually adds a finite inertia [33,52,53] that reduces the amplitude of DE mode at the sample surface and hence the scattering potential. A cutoff momentum k_c can take care of the exchange effect as follows [33,52,53]. When the exchange energy $\mu_0\gamma M_0\alpha_{\rm ex}k^2$ is one order of magnitude smaller than the dipolar one $\mu_0\gamma M_0$, i.e., $\alpha_{\rm ex}k_c^2 \gtrsim 0.1$, the exchange interaction can be disregarded. For YIG with $\alpha_{\rm ex} = 3\times10^{-16}$ [28,52,53], $k_c \gtrsim 5\times10^6 {\rm m}^{-1}$. With our film thickness $d = 3\times10^{-6}$ m, $k_c d \gtrsim 15$. Here, we focus on momenta $kd \simeq 4$, which implies still relatively weak coupling as well as absence of exchange effects.

For DE magnons with $\mathbf{k} = k_y\hat{\mathbf{y}}$, when $k_y d \gtrsim 2$, $\alpha_s(\omega_{\mathbf{k}}) \sim \sigma k_y$ and increases slowly with large R when $R \gtrsim d$. The inset in Fig. 4 shows these dependencies for typical parameters $H_z = M_0$ and $k_y d = 3$. The effect of the enhanced scattering potential by a large R [see Eq. (45)] is largely canceled by the simultaneous squeezing of the magnon scattering phase space (see Fig. 3). The small effect of an applied field H_z is caused by another cancellation of two effects: On one hand, the effective scattering potential contributed by the Zeeman perturbation [Eq. (37)] is proportional to H_z, while on the other hand the Lorentzian magnon spectral function broadens with H_z for constant α_0. As long as $|\mathbf{k}|d \gtrsim 1$, α_s does not depend strongly on the thickness of the film either, because the surface magnon wave function $m^{\mathbf{k}}_{x,y}(d/2) \propto \sqrt{k}$ [see Eq. (6)] and hence the local scattering potentials in Eqs. (31) and (37) do not depend significantly on the thickness of the sample. This also implies that the surface-induced damping of surface magnons in magnetic spheres is not expected to depend on a radius in the submillimeter range [14–17]. Also, surface damping only weakly depends on a bulk Gilbert damping when $\alpha_0 \ll \alpha_s$.

V. TRANSPORT OF SURFACE MAGNONS

Forward scattering is not as detrimental for transport as backscattering. Large differences in the single-particle and transport lifetimes of electrons therefore exist when the scattering potential is long range [36–38,54]. We may expect similar physics for DE-magnon transport in the linear response regime [36–38,54].

A. Linear response theory

The magnon number current $\mathbf{J}_m$ and magnon heat current $\mathbf{J}_Q$ respond to a magnon accumulation gradient that is parametrized by a spatially dependent temperature T and chemical potential μ_m. In linear response,

$$\begin{pmatrix}\mathbf{J}_m\\ \mathbf{J}_Q\end{pmatrix} = \begin{pmatrix}\overline{\mathcal{L}}^{(11)} & \overline{\mathcal{L}}^{(12)}\\ \overline{\mathcal{L}}^{(12)} & \overline{\mathcal{L}}^{(22)}\end{pmatrix}\begin{pmatrix}\nabla\mu_m\\ \nabla T/(k_BT)\end{pmatrix}, \tag{50}$$

where $\overline{\mathcal{L}}^{(ij)}$ are material response tensors [5,55]. Here we focus on transport by $\nabla\mu_m$ while $\nabla T = 0$, i.e., the magnon (number) conductivity $\overline{\mathcal{L}}^{(11)} \equiv \mathcal{L}$. In the static limit,

$${\rm Re}\mathcal{L}_{\alpha\alpha} = -\lim_{\omega\to0}{\rm Im}\frac{\Pi^{\rm ret}_{\alpha\alpha}(\omega)}{\omega}, \tag{51}$$

with $\alpha = \{y, z\}$.

$$\Pi^{\rm ret}_{\alpha\alpha}(\omega) = -i\int_{-\infty}^{\infty}dt'\Theta(t-t')e^{i\omega(t-t')}\langle[\hat{\jmath}^\dagger_\alpha(t), \hat{\jmath}_\alpha(t')]\rangle \tag{52}$$

is the retarded current-current correlation function. $\hat{\jmath}_\alpha = \sum_{\mathbf{k}} v^\alpha_{\mathbf{k}}\hat{\alpha}^\dagger_{\mathbf{k}}\hat{\alpha}_{\mathbf{k}}$ represents the magnon number current (not directly proportional to the spin current when magnon polarization is elliptic) operator in terms of the magnon group velocity $\mathbf{v}_{\mathbf{k}} \equiv \partial\omega_{\mathbf{k}}/\partial\mathbf{k}$. For DE magnons with momentum $\mathbf{k} = k_y\hat{\mathbf{y}}$,

$$v^y_{k_y} = \frac{(\mu_0\gamma M_0)^2 d}{4\omega_{k_y}}e^{-2k_yd} \tag{53}$$

with the frequency [7,9]

$$\omega_{k_y} = \sqrt{\omega_H^2 + \omega_H\omega_M + \omega_M^2\frac{1-e^{-2k_yd}}{4}}.$$

$v^y_{k_y}$ exponentially tends to zero with increasing k_y.

It is again convenient to calculate first the Matsubara Green function $\Pi_{\alpha\alpha}(i\omega_n)$ followed by analytical continuation $i\omega_n \to \omega + i\delta$ [36–38,54]. Then

$${\rm Re}\mathcal{L}_{\alpha\alpha} = \int_{-\infty}^{\infty}\frac{d\varepsilon}{2\pi}\left(-\frac{dn_B(\varepsilon)}{d\varepsilon}\right)P(\varepsilon-i\delta, \varepsilon+i\delta), \tag{54}$$

where $n_B(\varepsilon) \equiv (e^{\beta\varepsilon}-1)^{-1}$ and

$$P(\varepsilon-i\delta, \varepsilon+i\delta) = \sum_{\mathbf{k}} v^\alpha_{\mathbf{k}}\Gamma^\alpha_{\mathbf{k}}(\varepsilon-i\delta, \varepsilon+i\delta)G_{\mathbf{k}}(\varepsilon+i\delta) \times G_{\mathbf{k}}(\varepsilon-i\delta). \tag{55}$$

Here, $\Gamma^\alpha_{\mathbf{k}}$ is the vertex function, which in the ladder approximation satisfies the integral equation

$$\Gamma^\alpha_{\mathbf{k}}(\varepsilon-i\delta, \varepsilon+i\delta) = v^\alpha_{\mathbf{k}} + \sum_{\mathbf{k}'}\Gamma^\alpha_{\mathbf{k}'}(\varepsilon-i\delta, \varepsilon+i\delta)|\mathcal{B}_{\mathbf{k}\mathbf{k}'}|^2 \times G_{\mathbf{k}'}(\varepsilon+i\delta)G_{\mathbf{k}'}(\varepsilon-i\delta). \tag{56}$$

This integral equation is difficult to solve in general [36–38,54]. However, for DE magnons with momentum perpendicular to the magnetization, we can find an approximate solution for their transport perpendicular to the magnetization, i.e., $\mathcal{L}_{yy}$, with long-ranged surface roughness as follows.

We use the identity $G_{\mathbf{k}}(\varepsilon+i\delta)G_{\mathbf{k}}(\varepsilon-i\delta) = A_{\mathbf{k}}(\varepsilon)/[2\Delta_{\mathbf{k}}(\varepsilon)]$ with spectral function

$$A_{\mathbf{k}}(\varepsilon) = \frac{2\Delta_{\mathbf{k}}(\varepsilon)}{[\varepsilon-\omega_{\mathbf{k}}-{\rm Re}\,\Sigma_{\mathbf{k}}(\varepsilon)]^2+\Delta^2_{\mathbf{k}}(\varepsilon)} \tag{57}$$

and $\Delta_{\mathbf{k}}(\varepsilon) = -{\rm Im}\Sigma_{\mathbf{k}}(\varepsilon)$ being the total broadening by the intrinsic Gilbert damping and surface roughness [see Eq. (44)]. The spectral function appears in both Eqs. (55) and (56), indicating that $\omega_{\mathbf{k}} \approx \omega_{\mathbf{k}'} \approx \varepsilon$ when the broadening is small and $A_{\mathbf{k}}(\varepsilon) \to 2\pi\delta(\varepsilon-\omega_{\mathbf{k}})$. Both $\mathbf{k}$ and $\mathbf{k}'$ are nearly normal to the magnetization, as established in the previous sections (see Fig. 3). In other words, the DE magnons with momenta $\mathbf{k}$ are scattered mainly along the $\hat{\mathbf{y}}$ direction. Furthermore, for smooth surface roughness, the momentum transfer between DE modes is not very large. When writing $\Gamma^y_{\mathbf{k}}(\varepsilon-i\delta, \varepsilon+i\delta) = v^y_{\mathbf{k}}\gamma_{\mathbf{k}}(\varepsilon-i\delta, \varepsilon+i\delta)$, for $|\mathbf{k}|d \gtrsim 1$, using $v^y_{\mathbf{k}} \sim e^{-2k_yd}$

from Eq. (53) and expressing $|\mathcal{B}_{\mathbf{k}\mathbf{k}'}|^2 \sim Qk_yk'_ye^{-|\mathbf{k}'-k_y\hat{\mathbf{y}}|^2R^2/4}$ for nearly one-dimensional scattering,

$$F = \lim_{\varepsilon\to\omega_{\mathbf{k}}} \sum_{\mathbf{k}'} \frac{v^y_{\mathbf{k}'}}{v^y_{k_y}} \frac{|\mathcal{B}_{\mathbf{k}\mathbf{k}'}|^2}{(\omega-\omega_{\mathbf{k}'})^2+(\Delta_{\mathbf{k}'}(\varepsilon))^2}$$
$$\to \sum_{\mathbf{k}'} e^{-2(k'_y-k_y)d} e^{-|\mathbf{k}'-k_y\hat{\mathbf{y}}|^2R^2/4} \frac{Qk_yk'_y}{(\omega_{\mathbf{k}}-\omega_{\mathbf{k}'})^2+\Delta^2_{\mathbf{k}}}. \quad (58)$$

The first and second exponentials limit the scattering vectors $|k'_y-k_y| \lesssim 1/(2d)$ and $|k'_y-k_y| \lesssim 2/R$, respectively. When $2/R \lesssim 1/(2d)$ and hence $R \gtrsim 4d$, substituting the "mean value" of k'_y by k_y+1/R in the first exponential leads to

$$F \gtrsim e^{-2d/R} \sum_{\mathbf{k}'} \frac{|\mathcal{B}_{\mathbf{k}\mathbf{k}'}|^2}{(\omega_{\mathbf{k}}-\omega_{\mathbf{k}'})^2+\Delta^2_{\mathbf{k}}} = e^{-2d/R}, \quad (59)$$

where we used

$$\sum_{\mathbf{k}'} |\mathcal{B}_{\mathbf{k}\mathbf{k}'}|^2 \frac{1}{(\omega_{\mathbf{k}}-\omega_{\mathbf{k}'})^2+(\mathrm{Im}\,\Sigma_{\mathbf{k}})^2} = 1 \quad (60)$$

from the self-consistent Born approximation. $\gamma_{\mathbf{k}}$ therefore does not depend on $\mathbf{k}$ to leading order when $R \gtrsim 4d$. This allows application of the mean value theorem, which leads to $\gamma_{\mathbf{k}'} \approx \gamma_{\mathbf{k}}$. We arrive at the closed expression

$$\Gamma^y_{\mathbf{k}}(\varepsilon-i\delta,\varepsilon+i\delta) \approx v^y_{\mathbf{k}}(1-F)^{-1} \quad (61)$$

and

$$\mathrm{Re}\,\mathcal{L}_{yy} = \int_{-\infty}^{\infty} \frac{d\varepsilon}{2\pi}\left(-\frac{dn_B(\varepsilon)}{d\varepsilon}\right) \sum_{\mathbf{k}} \left(v^y_{\mathbf{k}}\right)^2 \frac{A_{\mathbf{k}}(\varepsilon)}{2\Delta^t_{\mathbf{k}}(\varepsilon)}, \quad (62)$$

where

$$2\Delta^t_{\mathbf{k}}(\varepsilon) = 2\Delta_{\mathbf{k}}(\varepsilon)\left[1-\sum_{\mathbf{k}'} \frac{v^y_{\mathbf{k}'}}{v^y_{\mathbf{k}}} \frac{A_{\mathbf{k}'}(\varepsilon)}{2\Delta_{\mathbf{k}'}(\varepsilon)} |\mathcal{B}_{\mathbf{k}\mathbf{k}'}|^2\right]. \quad (63)$$

We thus derived a relation between the lifetime broadening in Eq. (63) and the transport damping coefficient for the magnon propagating nearly perpendicular to the magnetization:

$$\alpha_t(\omega_{\mathbf{k}}) = \frac{2\Delta^t_{\mathbf{k}}}{\omega_{\mathbf{k}}} = \alpha_s(\omega_{\mathbf{k}})(1-F), \quad (64)$$

where F accounts for the backscattering contribution [36–38,54].

With $d = 3\ \mu$m, the suppressing factor (58) is calculated to be $F \gtrsim 0.61$ when $R = 12\ \mu$m, and $F \gtrsim 0.74$ when $R = 20\ \mu$m. α_s does not change much with larger R when $k_yd \gtrsim 2$ (see Fig. 4) and hence α_t decreases exponentially with increasing R. The transport of DE magnons perpendicular to the magnetization is therefore efficient for smooth surface roughness, i.e., when $R \gtrsim 4d$, even though their lifetime can be very short. For larger $\mathbf{k}$ or shorter-ranged roughness, i.e., $R \lesssim 4d$, $\alpha_t(\omega_{\mathbf{k}}) \lesssim \alpha_s(\omega_{\mathbf{k}})$ still holds, but the transport of DE magnons is not protected anymore because the group velocity and in-scattering of DE magnons exponentially decreases. We conclude that smooth surface roughness affects the transport of DE magnons much less than the large lifetime broadening suggests, which is caused by chirality and long-range disorder, which both favor strong forward scattering.

B. Chiral conductivity

As addressed in Sec. IV B, DE magnons propagating in opposite directions experience different scattering potential when the surface roughness is different at the two surfaces, which leads to different magnon conductivities when the in-plane magnetic field is reversed, i.e., $\overline{\mathcal{L}}^{ij}_{yy}(\mathbf{M}) \neq \overline{\mathcal{L}}^{ij}_{yy}(-\mathbf{M})$. The magnon conductivity (associated with the magnon number [55–57]) can be estimated from Eq. (62). In the weak scattering regime, the spectral function $A_{\mathbf{k}}(\varepsilon) \to 2\pi\delta(\varepsilon-\omega_{\mathbf{k}})$, and the spin conductivity reduces to the conventional form from the Boltzmann equation [55,57],

$$\mathcal{L} \triangleq \mathrm{Re}\,\overline{\mathcal{L}}^{(11)}_{yy} = \sum_{\mathbf{k}} \left(v^y_{\mathbf{k}}\right)^2 \frac{1}{2\Delta^t_{\mathbf{k}}}\left(-\frac{dn_B(\omega_{\mathbf{k}})}{d\omega_{\mathbf{k}}}\right), \quad (65)$$

where n_B is the Boltzmann distribution function. The spin Seebeck coefficient $\overline{\mathcal{L}}^{(12)}$ and magnon heat conductivity $\overline{\mathcal{L}}^{(22)}$ are obtained by replacing one or two magnon number-current operators $\hat{\jmath}_\alpha$ in Eq. (52) by the magnon energy-current operator $\hat{\jmath}^Q_\alpha = \sum_{\mathbf{k}} \hbar\omega_{\mathbf{k}} v^\alpha_{\mathbf{k}} \hat{\alpha}^\dagger_{\mathbf{k}} \hat{\alpha}_{\mathbf{k}}$ [38], leading to [38,55,57]

$$\mathrm{Re}\,\overline{\mathcal{L}}^{(12)}_{yy} = \sum_{\mathbf{k}} \left(v^y_{\mathbf{k}}\right)^2 \frac{\hbar\omega_{\mathbf{k}}}{2\Delta^t_{\mathbf{k}}}\left(-\frac{dn_B(\omega_{\mathbf{k}})}{d\omega_{\mathbf{k}}}\right) \approx \hbar\omega_{\mathrm{DE}}\mathcal{L}, \quad (66)$$

$$\mathrm{Re}\,\overline{\mathcal{L}}^{(22)}_{yy} = \sum_{\mathbf{k}} \left(v^y_{\mathbf{k}}\right)^2 \frac{\left(\hbar\omega_{\mathbf{k}}\right)^2}{2\Delta^t_{\mathbf{k}}}\left(-\frac{dn_B(\omega_{\mathbf{k}})}{d\omega_{\mathbf{k}}}\right) \approx (\hbar\omega_{\mathrm{DE}})^2\mathcal{L}. \quad (67)$$

where the approximation is allowed when conduction is dominated by the DE magnons with narrow bandwidth [7]. $v^y_{\mathbf{k}}$ can be estimated by Eq. (53) due to the "ridge"-like shape of the DE dispersion [7]. In Eq. (67), $\Delta^t_{\mathbf{k}} \equiv 1/(2\tau_{\mathbf{k}})$ is inversely proportional to the momentum scattering time $\tau_{\mathbf{k}}$. Magnon transport is thereby understood as magnon diffusion driven by the magnon-accumulation gradient parametrized by the temperature and chemical potential. In the relaxation-time approximation, the steady-state Boltzmann equation $\mathbf{v}_{\mathbf{k}} \cdot \nabla_{\mathbf{r}} f(\mathbf{k},\mathbf{r}) = -[f(\mathbf{k},\mathbf{r}) - n_B(\omega_{\mathbf{k}})]/\tau_{\mathbf{k}}$ for the distribution function $f(\mathbf{k},\mathbf{r})$ reconciles our results with those in Refs. [55,57] for bulk systems.

Figure 5 shows the magnetic-field dependence of the magnon conductivities $\mathcal{L}(\mathbf{M})$ and $\mathcal{L}(-\mathbf{M})$ at room temperature $T = 300$ K. When the upper surface is rough with $\sigma_u = 4\ \mu$m and $R = 12\ \mu$m but the lower surface is flat, we find $\mathcal{L}(-\mathbf{M}) \approx 3\mathcal{L}(\mathbf{M})$ in a YIG film with thickness $d = 3\ \mu$m, where $\mathcal{L}(\mathbf{M})$ and $\mathcal{L}(-\mathbf{M})$ are dominated by the DE magnons near the upper and lower surfaces, respectively. For momenta $|\mathbf{k}|d \gtrsim 1$, the scattering is chiral, so the upper surface roughness efficiently scatters the DE magnons near the upper surface, but does not affect the modes on the lower surface. Therefore, the spin conductivity changes when the in-plane magnetic field is reversed. However, we do not generate a short circuit even in the absence of all scattering at the lower surface since the DE magnons with relatively small momenta $|\mathbf{k}|d \lesssim 1$ on the lower surface are still scattered by the upper surface roughness. $\mathcal{L}$ decreases with increasing magnetic field because $\omega_{\mathbf{k}}$ increases and the freeze-out effect $dn_B(\omega_{\mathbf{k}})/d\omega_{\mathbf{k}} \propto 1/\omega^2_{\mathbf{k}}$. From the transport lifetime $\tau^t_{\mathbf{k}} \equiv 1/(2\Delta^t_{\mathbf{k}})$, we expect $\mathcal{L}^{-1} \propto \sigma(1-e^{-2d/R})$.

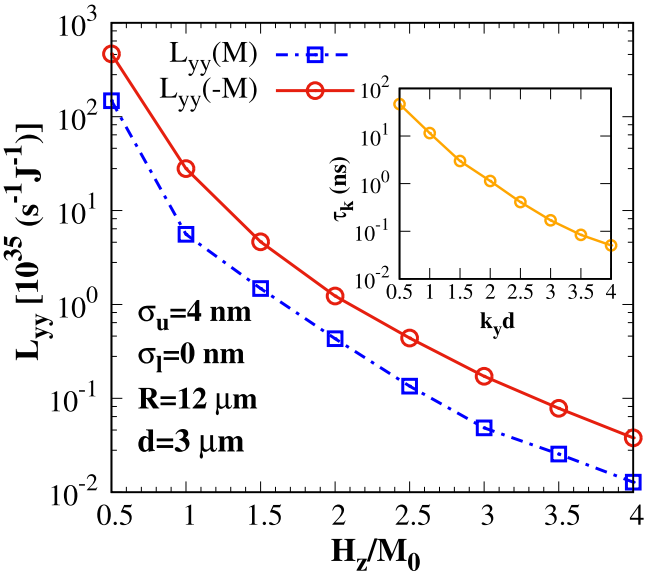

FIG. 5. Magnetic-field dependence of spin conductivities $L_{yy}(\mathbf{M})$ (blue dashed curve with squares) and $L_{yy}(-\mathbf{M})$ (red solid curve with circles) at room temperature, $T = 300$ K.

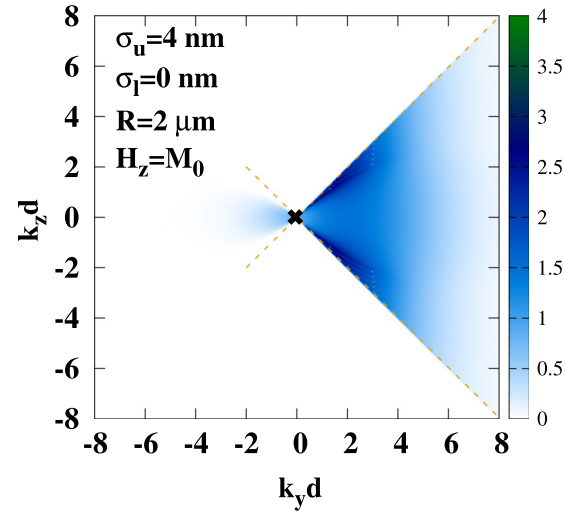

FIG. 6. Momentum dependence of the scattering potential $|\mathcal{B}_{\mathbf{k}K}|$ (in units of $10^{-8}\mu_0\gamma M_0$) between the Kittel mode (marked by a cross) and DE modes with wave vector $\mathbf{k}$. The orange dashed curves $k_z = \pm\sqrt{H_z/M_0}k_y$ are the equal-frequency contour of the DE and Kittel modes that define the boundary between surface and bulk modes [7].

We may compare the surface conductivity with that of the parallel channel of the bulk exchange modes with higher energy but larger group velocity. From the calculated bulk conductivity L_b at room temperature, in the film with $d = 3\mu$m, $\mathcal{L}' = L_b d \approx 5 \times 10^{41}(\mathrm{s\,J})^{-1}$ [57], about four orders in magnitude larger than the surface contribution. The spin conductivity contributed by the magnetostatic bulk magnons should be much smaller than $\mathcal{L}'$ because of their small group velocity. DE magnon channels can still be identified in transport by their chirality or by selective excitation.

Conductivities parametrize the ability for transport, here the magnon number, angular momentum, and energy. The magnon number and heat current can be directly obtained from the transport coefficients and Eq. (50) when the gradients are known. Often, conductivities can be expressed in terms of transport relaxation times $\tau_{\mathbf{k}}$ [36,38,54]. For magnon transport perpendicular to the magnetization [36,38,54,55,57],

$$\tau_{\mathbf{k}} \equiv \frac{1}{2\Delta^t_{\mathbf{k}}} = \frac{1}{\alpha_s(\mathbf{k})\omega_{\mathbf{k}}(1-F)}. \tag{68}$$

We plot the momentum dependence of the transport lifetime of the upper-surface DE magnons in the inset of Fig. 5 for the same parameters as the main panel. With increasing momentum, the transport lifetime decreases from nearly 100 ns to tens of picoseconds.

Pirro *et al.* [23] report a micromagnetic study of ultrathin films with a local strongly scattering defect, reporting a suppression of backscattering of magnons in the DE configuration far into the exchange regime. This result appears to be similar to ours, but it is difficult to compare these two very different approaches. Pirro *et al.* do not address the magnon lifetime or self-energy, which is important for experiments that study their spectral properties. Moreover, we are able to treat thick films in which the surface states are well developed, which are difficult to model by micromagnetism. We also focus on weak long-range correlated disorder in order to exclude scattering into volume exchange modes, which may reduce transport significantly when the spectra of surface and bulk modes overlap [23]. We plan to extend the present quasianalytical method to assess the thin-film regime and short-range scattering potentials by including the exchange interaction in a future study.

VI. EXCITATION OF SURFACE MAGNONS FROM SURFACE ROUGHNESS

For long-range disorder, the scattering of DE magnons with momenta $k_y\hat{\mathbf{y}}$ into bulk states close to the Kittel mode in energy is very inefficient, and we disregarded it completely in the discussion of the DE magnon lifetimes. Also, for the surface conductivity, the scattering into the Kittel mode contributes only in a very small region of momentum space. However, the inverse process, i.e., the scattering of bulk magnons into surface modes with finite k_z is allowed (see Fig. 6) [7]: The DE modes with momenta $\mathbf{k} = k_y\hat{\mathbf{y}}$ are well separated in energy and therefore cannot scatter elastically into bulk modes. On the other hand, the DE modes very close to the boundary between bulk and DE modes with significant k_z are nearly degenerate with the Kittel mode [7] and can be populated via surface roughness when the latter is excited by a *uniform* microwave field. DE magnon numbers on both sides of a film excited by the uniform microwave field differ when the roughness is asymmetric [11–13].

A. Model

We consider a subspace consisting of the Kittel modes and DE modes with momenta $\mathbf{k} = (0, k_y, k_z)$, with operators $\hat{\alpha}_K$ and $\hat{\alpha}_{\mathbf{k}}$ respectively, and interaction matrix elements $\mathcal{B}_{\mathbf{k}K}$. The Hamiltonian of noninteracting [34,35] magnons coupled to a uniform linearly polarized microwave field $H_x\hat{\mathbf{x}}$ with

frequency ω_d reads

$$\hat{H} = \omega_K \hat{\alpha}_K^\dagger \hat{\alpha}_K + \sum_{\mathbf{k}} \omega_{\mathbf{k}} \hat{\alpha}_{\mathbf{k}}^\dagger \hat{\alpha}_{\mathbf{k}} + \sum_{\mathbf{k}} (\mathcal{B}_{\mathbf{k}K} \hat{\alpha}_K^\dagger \hat{\alpha}_{\mathbf{k}} + \mathcal{B}_{\mathbf{k}K}^* \hat{\alpha}_{\mathbf{k}}^\dagger \hat{\alpha}_K) + 2g\hat{H}_x(t)(\hat{\alpha}_K + \hat{\alpha}_K^\dagger). \quad (69)$$

Here, $\hat{H}_x(t) = \hat{h}_x(0)e^{-i\omega_d t} + \hat{h}_x^\dagger(0)e^{i\omega_d t}$ is the magnetic-field operator in terms of photon operator $\hat{h}_x$, and $g = \mu_0 d\sqrt{2\gamma M_0/2}\, m_x^K$ arises from the Zeeman coupling between the Kittel mode and the uniform microwave magnetic field. The master equations for the magnon operators are obtained from the Heisenberg equation [35,43,44], augmented by the dampings Γ_K and $\Gamma_{\mathbf{k}}$:

$$\frac{d\hat{\alpha}_K}{dt} = -i\omega_K \hat{\alpha}_K - \Gamma_K \hat{\alpha}_K - i\sum_{\mathbf{k}} \mathcal{B}_{\mathbf{k}K} \hat{\alpha}_{\mathbf{k}} - ig\hat{H}_x(t), \quad (70)$$

$$\frac{d\hat{\alpha}_{\mathbf{k}}}{dt} = -i\omega_{\mathbf{k}} \hat{\alpha}_{\mathbf{k}} - \Gamma_{\mathbf{k}} \hat{\alpha}_{\mathbf{k}} - i\mathcal{B}_{\mathbf{k}K}^* \hat{\alpha}_K. \quad (71)$$

From Eq. (71), we obtain [35,43,44]

$$\hat{\alpha}_{\mathbf{k}}(t) = \hat{\alpha}_{\mathbf{k}}(0)e^{-i\omega_{\mathbf{k}}t - \Gamma_{\mathbf{k}}t} - i\mathcal{B}_{\mathbf{k}K}^* \int_0^t d\tau\, e^{-(i\omega_{\mathbf{k}} + \Gamma_{\mathbf{k}})(t-\tau)} \hat{\alpha}_K(\tau). \quad (72)$$

When the damping and excitation of the Kittel mode is weak, the evolution of $\hat{\alpha}_K$ is free $d\hat{\alpha}_K/dt \approx -i\omega_K \hat{\alpha}_K \approx -i\omega_d \hat{\alpha}_K$ for the small time interval $\Gamma_{\mathbf{k}}$:

$$\hat{\alpha}_K(\tau) \approx \hat{\alpha}_K(t)e^{i\omega_d(t-\tau)}, \quad (73)$$

inside the integral often referred to as "Markov approximation" [43,44]. At large times

$$\hat{\alpha}_{\mathbf{k}}(t) = \hat{\alpha}_{\mathbf{k}}(0)e^{-i\omega_{\mathbf{k}}t - \Gamma_{\mathbf{k}}t} + i\mathcal{B}_{\mathbf{k}K}^* \hat{\alpha}_K(t) \frac{1 - e^{(i\omega_d - i\omega_{\mathbf{k}} - \Gamma_{\mathbf{k}})t}}{i\omega_d - i\omega_{\mathbf{k}} - \Gamma_{\mathbf{k}}}, \quad (74)$$

which settles into the steady state

$$\hat{\alpha}_{\mathbf{k}}(t \to \infty) = \frac{-\mathcal{B}_{\mathbf{k}K}^* \hat{\alpha}_K(t \to \infty)}{\omega_{\mathbf{k}} - \omega_d - i\Gamma_{\mathbf{k}}}. \quad (75)$$

By substituting this into Eq. (70) for $t \to \infty$,

$$\frac{d\hat{\alpha}_K}{dt} = -i\omega_K \hat{\alpha_K} - \Gamma_K \hat{\alpha}_K - ig\hat{H}_x(t) + \sum_{\mathbf{k}} \frac{|\mathcal{B}_{\mathbf{k}K}|^2 \hat{\alpha}_K}{-i(\omega_{\mathbf{k}} - \omega_d) - \Gamma_{\mathbf{k}}}. \quad (76)$$

Using the rotating wave approximation [35,43,44],

$$\hat{\alpha}_K(t \to \infty) = \frac{-g\hat{h}_x(0)e^{-i\omega_d t}}{\omega_K - \omega_d - i\Gamma_K - \sum_{\mathbf{k}} \frac{|\mathcal{B}_{\mathbf{k}K}|^2}{\omega_{\mathbf{k}} - \omega_d - i\Gamma_{\mathbf{k}}}}. \quad (77)$$

From Eq. (75), the excited DE magnon population

$$\delta n_{\mathrm{DE}} \equiv \sum_{\mathbf{k}} \langle \hat{\alpha}_{\mathbf{k}}^\dagger \hat{\alpha}_{\mathbf{k}} \rangle = \rho_s \langle \hat{\alpha}_K^\dagger \hat{\alpha}_K \rangle, \quad (78)$$

where

$$\rho_s \equiv \sum_{\mathbf{k}} \frac{|\mathcal{B}_{\mathbf{k}K}|^2}{(\omega_{\mathbf{k}} - \omega_K)^2 + \Gamma_{\mathbf{k}}^2} \quad (79)$$

is the FMR excitation efficiency of the DE magnons.

B. Results

We computed the surface-roughness–assisted excitation of the DE magnons for YIG films with material parameters introduced in Sec. IV B. The disorder on the upper and lower surfaces is chosen to be asymmetric, $\sigma_u = 4$ nm and $\sigma_l = 0$, nm and the correlation length $R = 2\ \mu$m, as above. In Fig. 6, we plot the effective scattering potential $|\mathcal{B}_{\mathbf{k}K}|$ between the Kittel mode and DE modes with momentum $\mathbf{k}$ for $H_z = M_0$.

The Kittel mode couples dominantly with the DE modes with positive k_y, i.e., the ones propagating on the upper surface that is chosen to be rough, even though the microwave field is uniform [11–13]. The orange dashed lines $k_z = \pm\sqrt{H_z/M_0}k_y$ are the equal-frequency contours of the DE and Kittel modes that separate bulk and surface modes (see Sec. II).

The efficiency ρ_s of the surface-roughness–assisted excitation of DE magnons in Eq. (79) with the resonant excitation of Kittel mode $\omega_d = \omega_K$ is $\rho_s = 2.4\%$, 3.4%, 4.8% and 7.5% for $H_z = 0.5M_0$, M_0, $1.5M_0$, and $2M_0$, respectively. A significant number of DE magnons is excited during FMR and it increases with magnetic field. The excitation efficiency can be enhanced by rougher surfaces.

The FMR-excited DE magnons with momentum $|\mathbf{k}|d \lesssim 1$ are distributed by $|\mathcal{B}_{\mathbf{k}K}|^2/[(\omega_{\mathbf{k}} - \omega_K)^2 + \Gamma_{\mathbf{k}}^2]$. The denominator is small for the magnons close to the dark-blue regions in Fig. 6. These magnons are well localized to the film surface even when $|\mathbf{k}|d \lesssim 1$ with finite k_z and they are still chiral [7], which implies that with asymmetric surface roughness one surface is preferentially excited. These results can be tested by Brillouin light scattering spectra for films with different roughness, and help one to understand the heat conveyer effect [10] in recent experiments in which a uniform magnetic field was shown to generate chiral heat transport [11–13].

VII. SUMMARY

In conclusion, we investigated the effects of long-range, static surface roughness on the damping and excitation of surface magnons in thick magnetic films with in-plane magnetic fields. We reveal an additional damping channel for the surface magnons that strongly reduces the lifetime of surface magnons with wave number $k \gtrsim d^{-1}$, where d is the film thickness, possibly far above the bulk Gilbert damping. This indicates that the spectral features of surface magnons are smeared out by surface disorder. It is also bad news for cavity optomagnonics [58–61] with DE modes, since the strong dephasing by surface roughness suppresses the coupling to optical whispering gallery modes. On the other hand, transport of DE magnons is protected since scattering is dominantly in the forward direction, which is caused by their nearly circular polarization and unidirectional propagation. The surface roughness also mixes the Kittel and DE modes

quite efficiently, such that even a uniform microwave field can pump considerable amounts of surface magnons out of the magnetic order, which is observable by Brillouin light scattering experiments. Moreover, an asymmetry of the surface roughness on both sides of the film generates unbalanced distributions of the surface magnons and chirality during spin and heat transport.

The surface roughness may be also dynamic, i.e., is both space and time dependent, generated by thermal surface acoustic waves [62–64]. We will show in future work that our framework for the static surface roughness may be generalized to the dynamic one.

ACKNOWLEDGMENTS

This work is financially supported by the Nederlandse Organisatie voor Wetenschappelijk Onderzoek (NWO) as well as JSPS KAKENHI Grant No. 26103006. One of the authors (T.Y.) would like to thank Simon Streib for useful discussions.

[1] B. Lenk, H. Ulrichs, F. Garbs, and M. Münzenberg, Phys. Rep. **507**, 107 (2011).
[2] A. V. Chumak, V. I. Vasyuchka, A. A. Serga, and B. Hillebrands, Nat. Phys. **11**, 453 (2015).
[3] D. Grundler, Nat. Nanotechnol. **11**, 407 (2016).
[4] V. E. Demidov, S. Urazhdin, G. de Loubens, O. Klein, V. Cros, A. Anane, and S. O. Demokritov, Phys. Rep. **673**, 1 (2017).
[5] G. E. W. Bauer, E. Saitoh, and B. J. van Wees, Nat. Mater. **11**, 391 (2012).
[6] L. R. Walker, Phys. Rev. **105**, 390 (1957).
[7] R. W. Damon and J. R. Eshbach, J. Phys. Chem. Solids **19**, 308 (1961).
[8] A. Akhiezer, V. Baríakhtar, and S. Peletminski, *Spin Waves* (North-Holland, Amsterdam, 1968).
[9] D. D. Stancil and A. Prabhakar, *Spin Waves—Theory and Applications* (Springer, New York, 2009).
[10] T. An, V. I. Vasyuchka, K. Uchida, A. V. Chumak, K. Yamaguchi, K. Harii, J. Ohe, M. B. Jungfleisch, Y. Kajiwara, H. Adachi, B. Hillebrands, S. Maekawa, and E. Saitoh, Nat. Mater. **12**, 549 (2013).
[11] O. Wid, J. Bauer, A. Müller, O. Breitenstein, S. S. P. Parkin, and G. Schmidt, Sci. Rep. **6**, 28233 (2016).
[12] E. Shigematsu, Y. Ando, S. Dushenko, T. Shinjo, and M. Shiraishi, Appl. Phys. Lett. **112**, 212401 (2018).
[13] P. Wang, L. F. Zhou, S. W. Jiang, Z. Z. Luan, D. J. Shu, H. F. Ding, and D. Wu, Phys. Rev. Lett. **120**, 047201 (2018).
[14] A. Osada, R. Hisatomi, A. Noguchi, Y. Tabuchi, R. Yamazaki, K. Usami, M. Sadgrove, R. Yalla, M. Nomura, and Y. Nakamura, Phys. Rev. Lett. **116**, 223601 (2016).
[15] X. Zhang, N. Zhu, C.-L. Zou, and H. X. Tang, Phys. Rev. Lett. **117**, 123605 (2016).
[16] J. A. Haigh, A. Nunnenkamp, A. J. Ramsay, and A. J. Ferguson, Phys. Rev. Lett. **117**, 133602 (2016).
[17] S. Sharma, Y. M. Blanter, and G. E. W. Bauer, Phys. Rev. B **96**, 094412 (2017).
[18] S. Sharma, Y. M. Blanter, and G. E. W. Bauer, Phys. Rev. Lett. **121**, 087205 (2018).
[19] M. Sparks, R. Loudon, and C. Kittel, Phys. Rev. **122**, 791 (1961).
[20] R. Arias and D. L. Mills, Phys. Rev. B **60**, 7395 (1999).
[21] A. Y. Dobin and R. H. Victora, Phys. Rev. Lett. **92**, 257204 (2004).
[22] E. Schlömann, J. Appl. Phys. **41**, 1617 (1969).
[23] M. Mohseni, T. Bracher, Q. Wang, D. A. Bozhko, R. Verba, B. Hillebrands, and P. Pirro, arXiv:1806.01554.
[24] T. Yu and M. W. Wu, Phys. Rev. B **93**, 045414 (2016).
[25] L. D. Landau and E. M. Lifshitz, *Electrodynamics of Continuous Media*, 2nd ed. (Butterworth-Heinenann, Oxford, 1984).
[26] A. G. Gurevich and G. A. Melkov, *Magnetization Oscillations and Waves* (CRC, Boca Raton, FL, 1996).
[27] P. Hansen, J. Appl. Phys. **45**, 3638 (1974).
[28] S. Klingler, A. V. Chumak, T. Mewes, B. Khodadadi, C. Mewes, C. Dubs, O. Surzhenko, B. Hillebrands, and A. Conca, J. Phys. D **48**, 015001 (2015).
[29] R. Verba, G. Melkov, V. Tiberkevich, and A. Slavin, Phys. Rev. B **85**, 014427 (2012).
[30] C. Kittel, *Quantum Theory of Solids* (Wiley, New York, 1963).
[31] A. Kamra and W. Belzig, Phys. Rev. Lett. **116**, 146601 (2016).
[32] T. Holstein and H. Primakoff, Phys. Rev. **58**, 1098 (1940).
[33] B. A. Kalinikos, Sov. J. Phys. **24**, 718 (1981).
[34] H. Suhl, J. Phys. Chem. Solids **1**, 209 (1957).
[35] V. E. Zaharov, V. S. L'vov, and S. S. Starobinets, Sov. Phys. Usp. **17**, 896 (1975).
[36] A. A. Abrikosov, L. P. Gorkov, and I. E. Dzyaloshinski, *Methods of Quantum Field Theory in Statistical Physics* (Prentice Hall, Englewood Cliffs, NJ, 1963).
[37] A. L. Fetter and J. D. Walecka, *Quantum Theory of Many Particle Systems* (McGraw-Hill, New York, 1971).
[38] G. D. Mahan, *Many Particle Physics* (Plenum, New York, 1990).
[39] T. L. Gilbert, IEEE Trans. Magn. **40**, 3443 (2004).
[40] A. B. Migdal, Sov. Phys. JETP **34**, 996 (1958).
[41] L. Gor'kov, Sov. Phys. JETP **36**, 1364 (1959).
[42] T. Ando, A. B. Fowler, and F. Stern, Rev. Mod. Phys. **54**, 437 (1982).
[43] C. W. Gardiner and M. J. Collett, Phys. Rev. A **31**, 3761 (1985).
[44] A. A. Clerk, M. H. Devoret, S. M. Girvin, F. Marquardt, and R. J. Schoelkopf, Rev. Mod. Phys. **82**, 1155 (2010).
[45] J. L. Chen, C. P. Liu, T. Liu, Y. Xiao, K. Xia, G. E. W. Bauer, M. Z. Wu, and H. M. Yu, Phys. Rev. Lett. **120**, 217202 (2018).
[46] H. Chang, P. Li, W. Zhang, T. Liu, A. Hoffmann, L. Deng, and M. Wu, IEEE Magn. Lett. **5**, 6700104 (2014).
[47] A. Aqeel, I. J. Vera-Marun, B. J. van Wees, and T. T. M. Palstra, J. Appl. Phys. **116**, 153705 (2014).
[48] G. Srinivasan, C. E. Patton, and P. R. Emtage, J. Appl. Phys. **61**, 2318 (1987).
[49] P. A. Grünberg, Rev. Mod. Phys. **80**, 1531 (2008).
[50] Y. Hashimoto, S. Daimon, R. Iguchi, Y. Oikawa, K. Shen, K. Sato, D. Bossini, Y. Tabuchi, T. Satoh, B. Hillebrands, G. E. W. Bauer, T. H. Johansen, A. Kirilyuk, T. Rasing, and E. Saitoh, Nat. Commun. **8**, 15859 (2017).

[51] B. Velicky, S. Kirkpatrick, and H. Ehrenreich, Phys. Rev. **175**, 747 (1968).

[52] R. E. De Wames and T. Wolfram, Appl. Phys. Lett. **15**, 297 (1969).

[53] T. Wolfram and R. E. De Wames, Phys. Rev. Lett. **24**, 1489 (1970).

[54] H. Haug and A. P. Jauho, *Quantum Kinetics in Transport and Optics of Semiconductors* (Springer, Berlin, 1996).

[55] L. J. Cornelissen, K. J. H. Peters, G. E. W. Bauer, R. A. Duine, and B. J. van Wees, Phys. Rev. B **94**, 014412 (2016).

[56] C. Sun, T. Nattermann, and V. L. Pokrovsky, J. Phys. D: Appl. Phys. **50**, 143002 (2017).

[57] B. Flebus, K. Shen, T. Kikkawa, K. I. Uchida, Z. Qiu, E. Saitoh, R. A. Duine, and G. E. W. Bauer, Phys. Rev. B **95**, 144420 (2017).

[58] O. O. Soykal and M. E. Flatté, Phy. Rev. Lett. **104**, 077202 (2010).

[59] H. Huebl, C. W. Zollitsch, J. Lotze, F. Hocke, M. Greifenstein, A. Marx, R. Gross, and S. T. B. Goennenwein, Phy. Rev. Lett. **111**, 127003 (2013).

[60] Y. Tabuchi, S. Ishino, T. Ishikawa, R. Yamazaki, K. Usami, and Y. Nakamura, Phy. Rev. Lett. **113**, 083603 (2014).

[61] X. Zhang, C.-L. Zou, L. Jiang, and H. X. Tang, Phy. Rev. Lett. **113**, 156401 (2014).

[62] M. Weiler, L. Dreher, C. Heeg, H. Huebl, R. Gross, M. S. Brandt, and S. T. B. Goennenwein, Phys. Rev. Lett. **106**, 117601 (2011).

[63] R. Sasaki, Y. Nii, Y. Iguchi, and Y. Onose, Phys. Rev. B **95**, 020407(R) (2017).

[64] R. Verba, I. Lisenkov, I. Krivorotov, V. Tiberkevich, and A. Slavin, Phys. Rev. Appl. **9**, 064014 (2018).